CHAPTER 5

CHARACTERIZATION OF THE GROWN CRYSTALS

Contents

5.1 INTRODUCTION

It is obvious that there are no ideal crystals in reality and all crystals grown by any technique do contain some defects, impurities and inhomogeneities. But, since most of the physical properties are sensitive to the deviation from ideality, the characterization of the grown crystals becomes a necessity. A full characterization of a crystal is very time consuming and needs large instrumental efforts. The reliability, precision and speed of chemical, structural and defect characterization by physical techniques can be enhanced significantly by computer-based laboratory automation. Not only the physicist, but also the crystal grower should be most interested in characterization of the crystals grown, since it is important to correlate the quality of the crystal with the growth technique and the growth parameters. The demand of crystals of the highest quality is increasing, and only systematic characterization enables the crystal grower to optimize the growth parameters in order to obtain better crystals.

There are several definitions of "characterization". Elwell and Scheel (1) argued that

a single crystal may be characterized by a description of its chemical composition, of its structure, of its defects and of the spatial distribution of these three factors. A full characterization should also include determination of electronic and excited states of the chemical constituents of the material. In addition, the results of many physical measurements can assist a full description of a specific crystal. However, physical properties alone of a given crystal cannot sufficiently characterize a crystal. Even a set of various physical properties will not allow the unequivocal identification of a material except for elements and some simple compounds. Chemical and crystallographic data are obviously preferable for the identification of a material. Laudise (2) however pointed out that no crystal has so far been ever characterized fully. Roy (3) and Donnay and Fleischer (4) proposed that the minimum data desirable for the characterization of a crystal include the parameters like nominal chemical formula, chemical analysis for major constituents, deviation from stoichiometry, trace analysis homogeneity of major and minor constituents, colour, crystal habit, cleavage, twinning, refractive index, X-ray identification, three dimensional data on size, precision determination of lattice constants, etc. An excellent review of

characterization and on the potential, the sensitivity and the accuracy of the various characterization techniques has been compiled by a committee on Characterization of Materials, Materials Advisory Board, National Academy of Sciences, Washington D.C., (1967) (vide report AD 649 941). 1 Ref. 5

The purpose of this chapter is to present the results of the characterization of calcium molybdate crystals grown by flux cooling method (described in Chapter 4) by making the best use of the different techniques available in this laboratory.

5.2 EXPERIMENTAL, OBSERVATIONS AND DISCUSSION

5.2.1 Energy Dispersive Analysis of X-rays (EDAX)

The "Energy Dispersive Analysis of X-rays" (EDAX) is an inevitable tool to estimate the semi-quantitative chemical composition of crystals. The scanning transmission electron microscope (STEM), Philips EM 400 has the EDAX attachment. The principle in brief is : when a beam of electrons strikes a specimen, a fraction of the incident electrons excite the atoms of the specimen, which then emits characteristic X-rays whose wavelength and energy are strictly related to the atomic number of the elements excited in the electron microscope. The

analysis of the energy spectrum is carried out by the energy dispersive method, thus identifying the emitting elements due to their characteristic X-ray wavelengths.

The specimen, under study, was mounted on a Pt-Cu-Ni alloy stud using silver paste (obtained from Polaron Equipment Limited, Watford Herts, UK) so as to obtain a good electrical contact between the sample and the stud. A thin layer of carbon was then coated on both the sample and the stud, in vacuum (10^{-6} torr), using carbon arcs, to make the surface much more conducting. When the high vacuum was attained, after inserting the sample in EM 400 T, the electron beam was made to strike the sample. The energy dispersed X-ray spectrum of $CaMoO_4$ thus obtained is as shown in Fig. 5.1, where the abscissa is X-ray energy in KeV and the ordinate is the number of counts. The figure shows two distinct peaks which are identified (by comparison with standard recorded charts of the energies of all K and L lines corresponding to each element) as calcium (Ca) and molybdenum (Mo). Oxygen (O) in the specimen, however, could not be detected directly by this technique due to a limitation of the instrument. Nevertheless, using the method of oxide ratio, the oxygen content was obtained from the spectrum shown in Fig. 5.1. The absence of trace

elements is attributed to the quality of the flux-grown $CaMoO_4$ crystals.

5.2.2 X-ray diffraction

The powder photograph method in conjunction with the diffractometer was employed to calculate the 'd' values from '2θ' reflections of different (hkl) planes of the crystal. CuK_α radiation obtained through a Ni filter and from a tube operating at 700 VA was used and the specimen was scanned in the diffracting angular range $\theta = 7^\circ$ to 42° at the counter speed of 1° min^{-1}. The intensities were recorded on synchronously advancing strip chart. Figure 5.2 illustrates the X-ray powder diffractogram obtained with $CaMoO_4$ crystal using the Horizontal Counter Tube Goniometer HZG 3, Veb Freibeerger Prazisions Mechanic - Carl Zeiss Jena equipment. The different 'd' values obtained from this are given in Table 5.1. The unit cell parameters, determined from these data, agreed closely well with the values reported in the literature (5). The unit cell dimension are :

$$a = b = 5.215\ \text{Å}, \quad c = 11.43\ \text{Å}$$

$$\alpha = \beta = \gamma = 90^\circ,$$

the crystal belongs to tetragonal system having space

Table 5.1 'd' values obtained from X-ray powder diffractogram of $CaMoO_4$ crystallites

Sr. No.	θ	2θ	'd' calculated	'd' ASTM	hkl
1.	9.4	18.8	4.719	4.76	101
2.	14.4	28.8	3.099	3.10	112
3.	15.65	31.3	2.858	2.86	004
4.	17.2	34.4	2.607	2.61	200
5.	19.7	39.4	2.287	2.290	211
6.	20.0	40.0	2.254	2.262	114
7.	23.6	47.2	1.926	1.929	204
8.	24.65	49.3	1.848	1.848	220
9.	27.2	54.4	1.687	1.694	116
10.	27.6	55.2	1.664	1.635	215
11.	29.1	58.2	1.585	1.588	312
12.	32.5	65.0	1.435	1.438	321
13.	38.2	76.4	1.247	1.249	315

group C_{4h}^{6}.

The perfect crystallinity of the grown products was identified with the help of Laue back reflection photograph such as the one shown in Fig. 5.3 for (011) face. The photograph shows distinct spot pattern pertaining to the characteristic two fold symmetry of the face, in good conformity with single crystallinity.

5.2.3 Differential thermogravimetric analysis (DTA)

This technique provides the analyst with a quantitative measure of any weight change with time or temperature due to such transition as dehydration or decomposition.

DTG analysis was done on the crystalline powder of $CaMoO_4$ between 50°C to 960°C employing a heating rate of 15°C per minute. No weight change was encountered throughout the temperature range studied. The typical DTA curve obtained is shown in Fig. 5.4, which reveals that the substance does not undergo any phase change during heating upto almost 1000°C.

5.2.4 Magnetic behaviour

The measurement of magnetic susceptibility

of the crystals was carried out using Faraday's Gouy method (6). The apparatus used for the purpose has already been described (Fig. 3.7) in chapter 3. The finely powdered crystals were packed into a glass tube of uniform cross section. This sample container was then suspended from one arm of the sensitive balance by a non-magnetic wire so that its axis remains vertical. Now the container was hung in between two powerful electromagnetic pole pieces of the Gouy's balance, of sensitivity 10^{-5} g. The container was weighed with and without the magnetic field. The field was varied by changing the current passing through the coils and each time a change in weight of the sample was noted. The experiment was repeated several times and the average change in weight was found out. The susceptibility χ_g of the substance was then calculated using the formula

$$\chi_g = \frac{KV + \beta\, dW}{W} \qquad (5.1)$$

where K = volume susceptibility of air, 0.029×10^{-6}

V = volume of water, 0.00699 for 5.7 K Gauss and 0.00465 for 7.8 K Gauss.

β = tube constant, 1.457×10^{-5} for 5.7 K Gauss and 1.453×10^{-5} for 7.8 K Gauss.

dW = the apparent change in weight of the sample, in gm.

W = weight of the sample, in gm.

The magnetic susceptibility χ_g of the $CaMoO_4$ was found to be -8.9327×10^{-8} emu/mole and -16.134×10^{-8} emu/mole with 5.7 K Gauss and 7.8 K Gauss respectively and the average molar magnetic susceptibility χ_m of the crystals was found to be -1.9267×10^{15} μ_B and -3.4800×10^{15} μ_B with 5.7 K Gauss and 7.8 K Gauss respectively. The negative sign signifies the characteristic diamagnetism prevailing in the crystal.

5.2.5 Infrared spectral analysis

The IR spectrum of $CaMoO_4$ was obtained using PERKIN-ELMER 983 spectrophotometer in the range of 300-4000 cm^{-1} and is shown in Fig. 5.5. We are inclined to suggest that the band at 433 cm^{-1} may be due to the dimetal-oxygen vibration. This is in agreement with the view of Dasent and Waddington (7) that in XO_4-type compounds the band at 325 cm^{-1} appears strongly in the infrared spectra, because the lowering of the symmetry and the degenerate vibrations often split and Raman active modes become infrared active in

crystalline state. Further, that the lattice water absorbs at the band 3431 cm^{-1} may be due to antisymmetric and symmetric O-H stretching modes (8) and at 1625 cm^{-1} is due to the H-O-H stretching mode. These bands are seen due to the medium KBr in the water-free compound.

The weak band at 1427 cm^{-1} and 2921 cm^{-1} show conspicuously the presence of KBr region (9) but the distinct, strong band observed at 813 cm^{-1} may be due to the presence of Mo in the compound. The band at 2328 cm^{-1} may be due to the impurity present by inclusion of flux; that this band is most feeble implies little occlusion of the flux particles in the growing matrix and hence perfection of the growth product.

5.2.6 Growth inhomogeneities

It seems to be widely accepted that striations in crystals grown from high temperature solutions arise from temperature fluctuations caused either by insufficient temperature control or by the convective instability. Striations are a common observation in a variety of crystals grown by the flux method (10-15). The occasionally observed striations, such as shown in Fig. 5.6, found on the as-grown (011)

faces of $CaMoO_4$ are believed to be due to self-existing variations in growth rate, that arose from the oscillations in temperature.

The fact that the presence of occluded flux too, however small, cannot be denied in crystals is evidenced to in Fig. 5.7 showing the existence of growth hillocks on impurity sites on the as-grown (011) faces. These hillocks, as also those of Fig. 5.8, may appear to be connected with screw dislocation sites but they have been identified by the selective etchant to have nondislocation origin. The hillocks in Fig. 5.8 give the illusion of a Frank-Read source operative in these crystals, but again they are found to have been formed by simply crowding and bunching of growth layers; they are the true manifestation of layer mechanism of growth of crystals. Normally, if the supersaturation is lowered below the value which can promote corner and edge nucleation, the characteristic features seen on most crystals are the growth hillocks presumably formed by a layer-bunching and crowding process, which give rise to the relatively thick layers visible under an optical microscope. The Fig. 5.8 clearly illustrates the modification of growth layers as the two and the three hillocks tend to coalesce. This figure is the

micrograph of a $CaMoO_4$ crystal on the surface of which the concentration of hillocks is higher at the crystal edges due to the higher local supersaturation. As growth continues at a stable rate, the concentration of hilloks near the edges decreases and so edge growth becomes less significant.

5.2.7 Miscellaneous characteristics

The different characteristics studied on $CaMoO_4$ crystals by using a variety of other techniques have been summarised in Table 5.2.

5.3 CONCLUSIONS

1. The grown crystals of calcium molybdate have been sufficiently characterised.
2. Differential thermogravimetric analysis (DTA) shows no phase transformation of crystals in the studied temperature range ($50^{o}C$-$960^{o}C$).
3. Calcium molybdate possesses diamagnetic susceptibility, the value of molar susceptibility being $-1.9267 \times 10^{15}\ \mu_B$ and $-3.48 \times 10^{15}\ \mu_B$, with 5.7 K Gauss and 7.8 K Gauss, respectively.
4. Fluctuations in furnace temperature are likely to cause surface inhomogeneities.

Table 5.2 Some properties studied of $CaMoO_4$ crystals

Sr. No.	Property studied	Result
1.	Maximum size, (mm)	12
2.	Colour	Opaque to transparent
3.	Habit	Bipyramidal
4.	Pycnometer density, g. ml^{-1}	4.136
	X-ray density, $g.ml^{-1}$	4.272
5.	Cleavage	(001) distinct
6.	Hardness on Mohs scale	
	(011) as-grown plane	5.25
	(001) cleaved plane	4.83
7.	Dielectric constant (ϵ') at 1 KHz and 25°C	28.61
8.	D.C. Electrical conductivity, σ (Ω^{-1} cm^{-1}) at 40°C	2.5×10^{-12}

REFERENCES

1. D. Elwell and H. J. Scheel. (1975)
"Crystal Growth from High-Temperature Solution", (Academic Press, London-New York-San Francisco) P. 471.

2. R. A. Laudise. (1975)
"Crystal Growth and Characterization" (Eds. R. Ueda and J. B. Mullin, North-Holland, Amsterdam) Ch. 19, p. 225.

3. R. Roy. (1965)
Physics Today, 18, 71.

4. G. Donnay and M. Fleischer. (1970)
Am. Min., 55, 1017.

5. Powder Data File. (1967)
(American Society for Testing and Materials, Philadelphia, Pennsylvania)
File No. 7-212.

6. L. F. Bates. (1951)
Modern Magnetism, Cambridge University Press, London, p. 15.

7. W. E. Dasent and T. C. Waddington. (1960)
J. Chem. Soc., 24-29, 3350.

8. M. Kobayashi and J. Fujita. (1953)
J. Chem. Phys., 23, 1354.

9. Foil A. Miller and Charles S. Wilkins. (1952)
J. Analytical Chem., 24, 1253.

10. A. I. Landau. (1958)
Phys. Met. Metallogr., 6, 132.

11. R. A. Lefever, A. B. Chase and
J. W. Torpy. (1961)
J. Am. Ceram. Soc., 44, 141.

12. E. A. D. White and J. W. Brightwell. (1965)
Chem. Ind., 39, 1662.

13. A. B. Chase. (1968)
J. Am. Ceram. Soc., 51, 507.

14. E. A. Giess, D. C. Cronemeyer, L. L. Rosier
and J. D. Kuptsis. (1970)
Mat. Res. Bull., 5, 495.

15. B. M. Wanklyn. (1975)
"Crystal Growth" (B. R. Pamplin Ed.)
Pergamon, Oxford.

Fig. 5.1 Video-display of X-ray energy dispersion of the grown crystal.

Fig. 5.3 Back reflection Laue photograph of (011) face of $CaMoO_4$ crystal.

Video display of X-ray energy dispersion of the grown crystal.

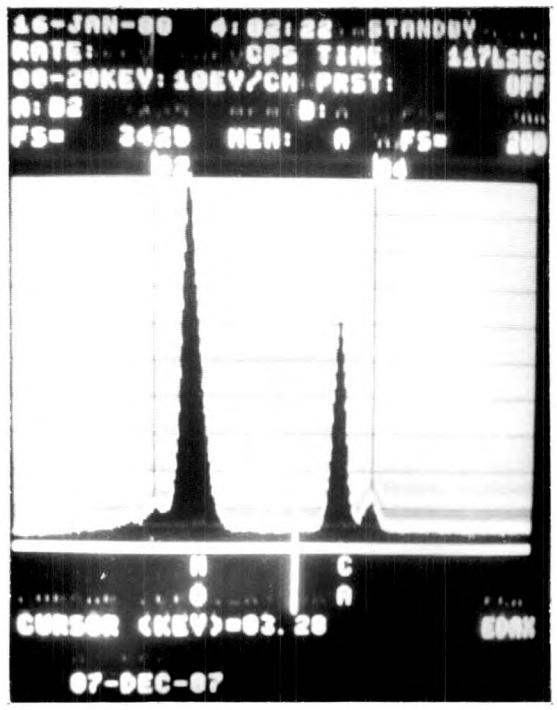

Fig.5.1

B

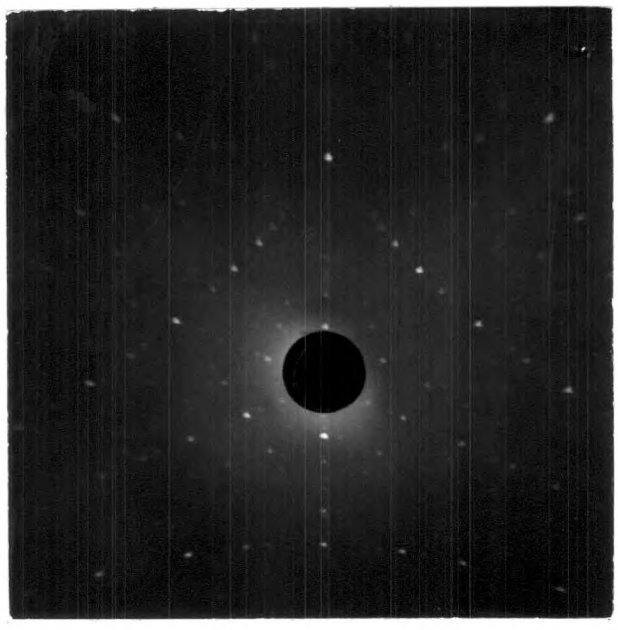

Fig. 5.3

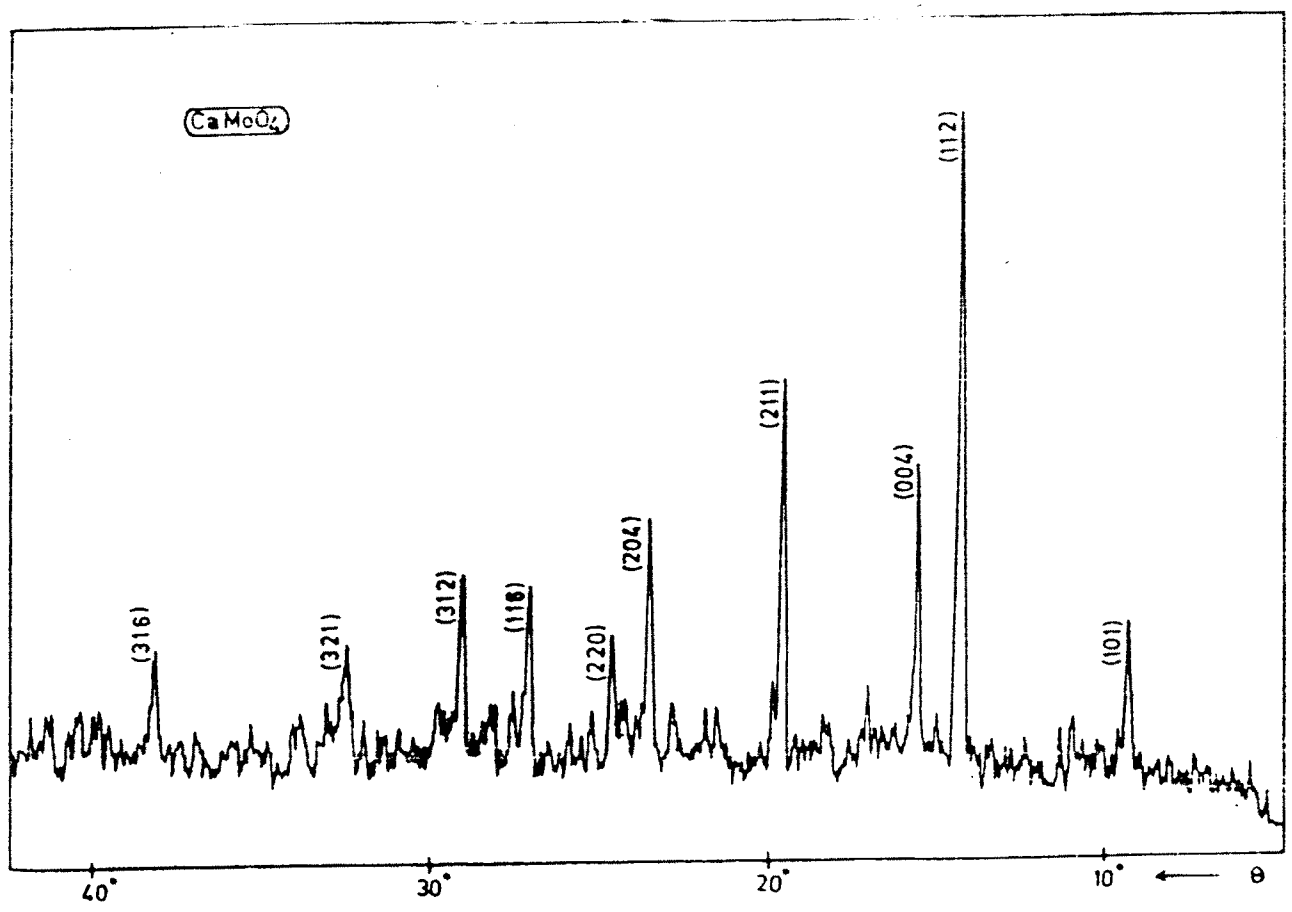

Fig. 5.2 X-ray powder diffractogram trace of $CaMoO_4$ crystals.

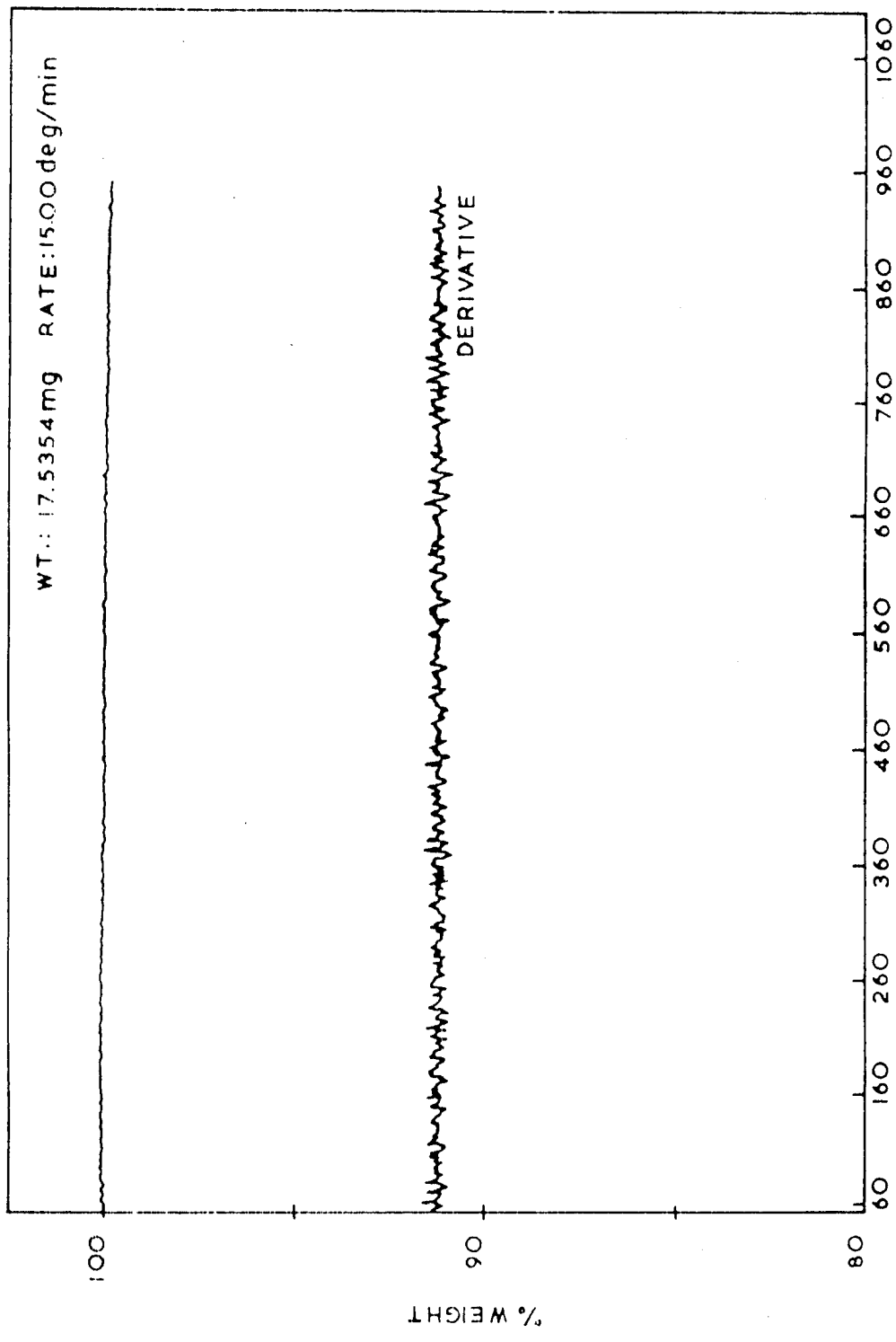

Fig. 5.4 The typical DTG analysis curve obtained for $CaMoO_4$ crystal.

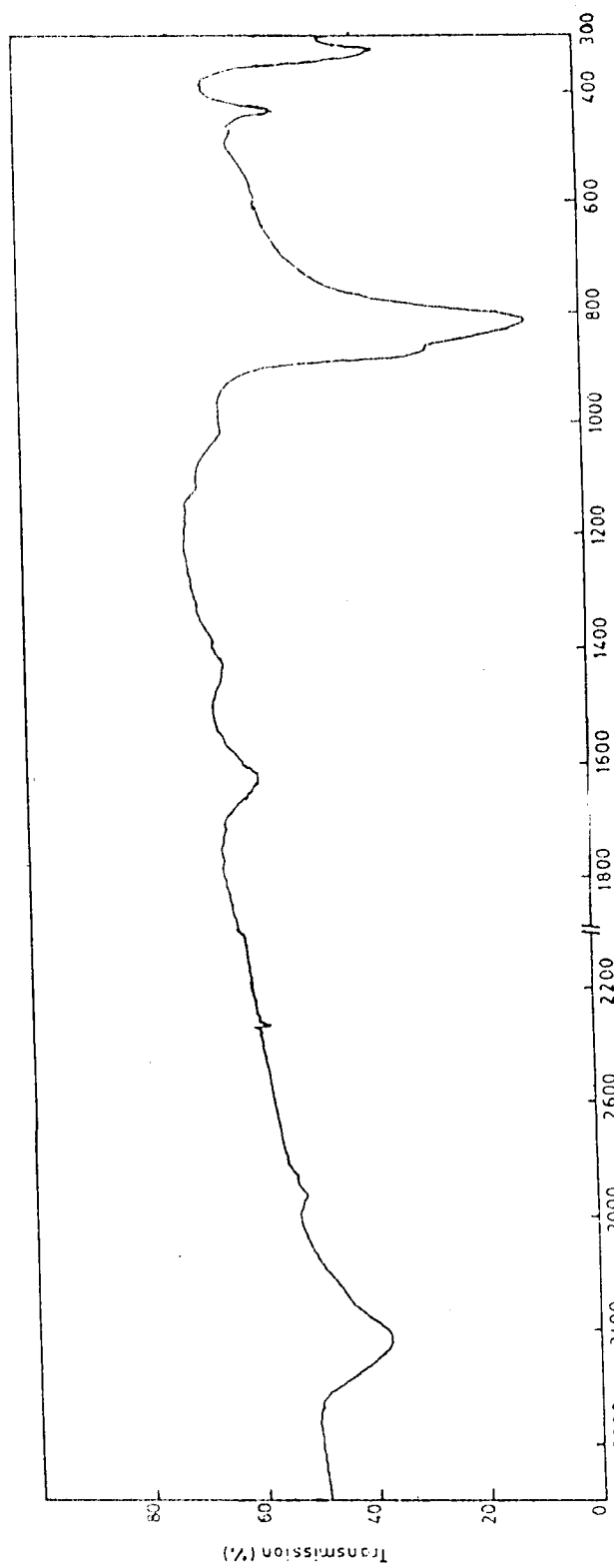

Table 5.5 An IR spectrum obtained for $CaMoO_4$ crystal.

Fig. 5.6 Striations observed on as-grown surface. X 170.

Fig. 5.7 Growth hillocks observed on as-grown faces of $CaMoO_4$ crystal. X 340.

Fig. 5.8 Growth hillocks observed on as-grown faces of $CaMoO_4$ crystal. X 340.

Striations observed on as-grown surface. X 170.

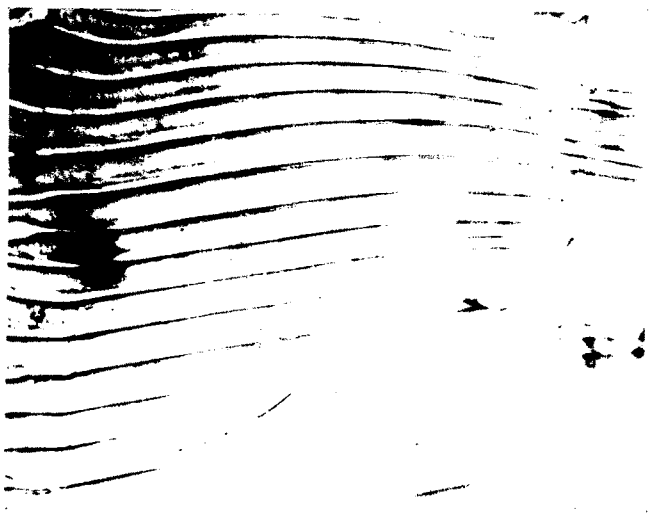

Fig. 5.6

Growth hillocks observed on as-grown faces of $CoMoO_4$ crystal. X 340.

Fig. 5.7

Growth hillocks observed on as-grown face of $CaMoO_4$ Crystal. X 340.

Fig. 5.8